

## Cluster approach to spontaneous fission of even-even isotopes of U, Pu, Cm, Cf, Fm, No, Rf, Sg, and Hs

I. S. Rogov,<sup>1,2</sup> G. G. Adamian,<sup>2</sup> and N. V. Antonenko<sup>1,2</sup>

<sup>1</sup>Joint Institute for Nuclear Research, 141980 Dubna, Russia

<sup>2</sup>Tomsk Polytechnic University, 634050 Tomsk, Russia



(Received 17 June 2021; accepted 30 August 2021; published 15 September 2021)

For even isotopes of nuclei U, Pu, Cm, Cf, Fm, No, Rf, Sg, and Hs, spontaneous fission and  $\alpha$ -decay half-lives are calculated within the dinuclear system model and compared with existing experimental data. Cluster radioactivity half-lives are also described for even U, Pu, and Cm isotopes. All these processes are considered for the evolution of a nucleus in the charge (mass) asymmetry coordinate and in the relative distance between the centers of clusters formed. The important roles of the driving potential and mass parameter in the charge asymmetry coordinate are shown for spontaneous fission. The global isotopic trends of spontaneous fission and  $\alpha$ -decay half-lives are studied. Drastic changes in the functional dependence of spontaneous fission half-life on the neutron number and in the absolute values of half-lives in the U–No and Rf–Hs nuclear groups are explained.

DOI: [10.1103/PhysRevC.104.034618](https://doi.org/10.1103/PhysRevC.104.034618)

### I. INTRODUCTION

The enhanced stability against spontaneous fission (SF) for Fm and No isotopes with the magic neutron number  $N = 152$  and the absence of this effect for nuclei beyond Lr are well recognized in many experiments [1–5]. The SF half-lives are not much different from each other for the isotopes  $^{256,258,260}\text{Rf}$  with  $N = 152, 154,$  and  $156$ . In contrast, a strong loss in the stability against SF occurs from  $N = 152$  to  $N = 150$  in Rf, Fm, and No isotopes, but not in lighter elements [6]. For nucleus  $^{260}\text{Rf}$  ( $^{256}\text{Rf}$ ), the measured half-life is about  $10^6$  ( $10^4$ ) times longer (shorter) than that expected from the extrapolation of experimental data for nuclei with the charge numbers  $Z < 103$  [6]. The drastic decline (by roughly seven orders of magnitude) of the SF half-lives from  $^{254}\text{No}$  ( $T_{1/2} = 3 \times 10^4$  s) to  $^{256}\text{Rf}$  ( $T_{1/2} = 6.4 \times 10^{-3}$  s) is especially striking because the behavior of the experimental  $Q_\alpha$  values for isotopes of Rf does not indicate the disappearance of the deformed neutron subshell at  $N = 152$ . It is generally assumed that this effect is mainly caused by the decreasing outer fission barrier below the ground state energy and consequently a reduction of the total width of the fission barrier [7]. The strong decrease in half-life from  $^{256}\text{Fm}$  to  $^{258}\text{Fm}$  is explained in two ways: the disappearance of the second saddle point in the potential barrier or the reduction of the mass parameter for fission [5,8–10]. So, a thorough explanation of the trend of SF half-lives of Fm, No, and Rf isotopes is required for a complete understanding of the fission process and, correspondingly, for future research on heavy and superheavy nuclei [11–13].

For the heaviest nuclei, the calculations of SF half-life were performed using the macroscopic-microscopic and self-consistent mean-field approaches [14–17]. The quadrupole and octupole moments are assumed to be relevant collective coordinates driving the nucleus to fission. These approaches

describe quite well the isotopic trends of  $T_{1/2}$ , for example, the enhanced stability of Fm and No at  $N = 152$  and of Sg and Hs at  $N = 162$ , but fail to reproduce the absolute values of lifetimes for many nuclei [6]. This means that the relative changes of the fission barriers are correct but the heights and thicknesses have to be further examined.

The model presented here belongs to the cluster type [18–39]. The ground state of the nucleus is assumed to have a small admixture of cluster-state components [40–45]. Here the cluster state means two touching nuclei or a dinuclear system (DNS). The total wave function of the nucleus is expressed by a superposition of cluster and clusterless components. The model [46] was developed to describe simultaneously the  $\alpha$  decay, cluster radioactivity (CR), and SF. All these processes were considered for the evolution of the system in the collective coordinates of charge  $\eta_Z$  (mass  $\eta$ ) asymmetry and in the relative distance  $R$  between the centers of clusters. Calculating the penetrability of the barrier in the nucleus-nucleus potential, the probability of the DNS decay in  $R$  is taken into consideration. The decays of almost symmetric DNS configurations are attributed to the SF. Indeed, the SF mainly occurs from the DNS configurations corresponding to the minima (deeper than the ground-state energy) of the driving potential which is the DNS potential energy as a function of  $\eta_Z$  or  $\eta$ .

In Sec. II, we discuss the cluster model of the spontaneous fission process. This model is employed in Sec. III to calculate the spontaneous fission half-lives of even-even heavy nuclei with the charge numbers  $Z = 90$ – $108$ . We analyze the isotopic trends of half-lives and compare them with existing experimental data. The stabilization of nuclei against spontaneous fission is discussed. The roles of potential energy and mass parameter in the spontaneous fission are studied. Finally, we summarize our results in Sec. IV.

## II. MODEL

Fission processes are considered here within the DNS model. In this model, the cluster formation with charge number  $Z_L \geq 2$  is described as the evolution of the system in the charge asymmetry coordinate

$$\eta_Z = \frac{Z_H - Z_L}{Z_H + Z_L}. \quad (1)$$

Here,  $Z_i$  ( $A_i$ ), where  $i = L, H$ , is the charge (mass) number of the  $i$ th cluster and  $Z = Z_L + Z_H$  ( $A = A_L + A_H$ ) is the total charge (mass) number of the DNS. The mass asymmetry coordinate  $\eta = (A_H - A_L)/(A_H + A_L)$  is assumed to be strongly related to  $\eta_Z$  by the condition of the potential energy minimum. Indeed, at given  $\eta_Z$  the DNS potential energy as a function of  $\eta$  has a well-defined minimum. So, the spreading in  $\eta$  is small at each  $\eta_Z$ . The decay of the formed DNS is considered as a motion of the DNS in the relative distance  $R$ .

Thus, the probability of finding two clusters  $L$  and  $H$  at given  $\eta_Z$  is proportional to the leakage of the ground-state wave function in  $R$  at this  $\eta_Z$ . To simplify the description of cluster decay [21–38], the process is usually divided into two independent stages: Forming the cluster state or DNS, and its decay in the  $R$  coordinate. Here, the decay process in terms of the DNS [45] is also divided into two stages and the total width of the decay is written as

$$\Gamma_L = \frac{\hbar\omega_0}{\pi} S_L P_L, \quad (2)$$

where  $S_L$  and  $P_L$  are the probabilities of DNS formation and decay, respectively;  $\omega_0$  is the frequency of zero-point vibration in the  $\eta_Z$  coordinate near the mononucleus state ( $\eta_Z \approx 1$ ). The value of  $\hbar\omega_0$  is equal to the distance between the ground and the first excited states of the DNS vibrating in  $\eta_Z$ .

The value of  $S_L$  is determined by solving the stationary Schrödinger equation

$$H\Psi_n(\eta_Z) = E_n\Psi_n(\eta_Z), \quad (3)$$

where the collective Hamiltonian

$$H = -\frac{\hbar^2}{2} \frac{\partial}{\partial \eta_Z} (B^{-1})_{\eta_Z} \frac{\partial}{\partial \eta_Z} + U(R, \eta_Z) \quad (4)$$

contains the inertia coefficient  $(B^{-1})_{\eta_Z}$  and the potential energy  $U(R, \eta_Z)$ .

The DNS potential energy [47]

$$U(R, \eta_Z, \Omega) = V(R, \eta_Z, \Omega) - (Q_M - Q_L - Q_H) \quad (5)$$

is referred to as the driving potential. Here  $Q_M$  is the mass excess of the parent nucleus and  $Q_L, Q_H$  are the mass excesses of the nuclei forming the DNS. The driving potential for the nucleus  $^{258}\text{No}$  is shown in Fig. 1. The tip-tip orientation of axial symmetric nuclei is taken in the calculations of driving potentials because it provides the minimum of the potential energy of the DNS considered. To come to the potential minimum of the depth  $U_m$  at  $\eta_Z \approx 0.2$  for SF, the DNS should pass through a barrier of height  $U_b$  and width  $w_{\eta_Z}$ .

The nucleus-nucleus interaction potential  $V$  in Eq. (5) consists of three types of interaction,

$$V(R, \eta_Z, \Omega) = V_C(R, \eta_Z) + V_N(R, \eta_Z) + V_r(R, \eta_Z, \Omega), \quad (6)$$

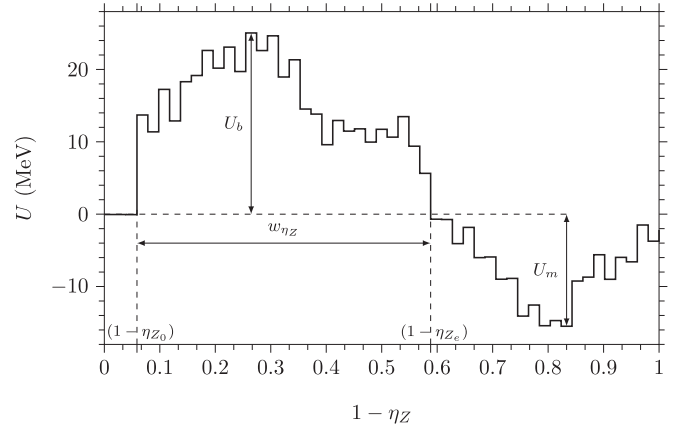


FIG. 1. Driving potential for  $^{258}\text{No}$ . The fission barrier in  $\eta_Z$  is characterized by the height  $U_b$  and the width  $w_{\eta_Z}$ . The depth of the potential minimum for SF is denoted by  $U_m$ . The tip-tip orientation of nuclei is taken in the DNS.

the Coulomb  $V_C$ , nuclear  $V_N$ , and the centrifugal  $V_r = \hbar^2\Omega(\Omega + 1)/(2\mathfrak{I})$  [where  $\mathfrak{I}$  is the moment of inertia of DNS] potentials. Here we consider the decays of even-even nuclei in the case of zero orbital angular momentum  $\Omega$ .

The Coulomb potential  $V_C$  is calculated as

$$V_C = \frac{e^2 Z_L Z_H}{R} \left( 1 + \frac{3}{5R^2} \sum_{i=L,H} R_i^2 \beta_{2i} Y_{20}(\theta_i) + \frac{12}{35R^2} \sum_{i=L,H} [R_i \beta_{2i} Y_{20}(\theta_i)]^2 \right), \quad (7)$$

where  $\beta_{2i}$  are the parameters of quadrupole deformation. In our calculations, we employ the experimental values of  $Q_L$  and  $Q_H$  from Ref. [48] and the values of the quadrupole deformation parameters from Ref. [49]. If the relevant experimental data are not available, we take the calculated values from Ref. [50]. The shape of each cluster is described as

$$R_i(\theta) = r_{0i} A_i^{1/3} [1 + \beta_{2i} Y_{20}(\theta)].$$

The nuclear part  $V_N$  of the interaction potential is calculated in the double folding form,

$$V_N = \int \rho_H(r_H) \rho_L(R - r_L) F(r_H - r_L) dr_H dr_L, \quad (8)$$

where the density-dependent nucleon-nucleon forces

$$F(r_H - r_L) = C_0 \left[ F_{\text{in}} \frac{\rho(r_H)}{\rho_0} + F_{\text{ex}} \left( 1 - \frac{\rho(r_H)}{\rho_0} \right) \right] \delta(r_H - r_L)$$

are folded with the nucleon densities  $\rho_H(\mathbf{r}_H)$  and  $\rho_L(\mathbf{R} - \mathbf{r}_H)$ . Here

$$F_{\text{in,ex}} = \xi_{\text{in,ex}} + \xi'_{\text{in,ex}} \frac{A_L - 2Z_L}{A_L} \frac{A_H - 2Z_H}{A_H}$$

and  $\rho(\mathbf{r}_H) = \rho_H(\mathbf{r}_H) + \rho_L(\mathbf{R} - \mathbf{r}_L)$ . The constants  $\xi_{\text{in}} = 0.09$ ,  $\xi_{\text{ex}} = -2.59$ ,  $\xi'_{\text{in}} = 0.42$ ,  $\xi'_{\text{ex}} = 0.54$ ,  $C_0 = 300$  MeV fm<sup>3</sup> are from Ref. [51]. We take the spatial axial

symmetric nucleon density in the form

$$\rho_{L,H}(\mathbf{r}) = \frac{\rho_0}{1 + \exp(|\mathbf{r} - \mathbf{R}_{L,H}|/a_{L,H})}, \quad (9)$$

where  $\rho_0 = 0.17 \text{ fm}^{-3}$  and  $a_{L,H}$  stands for the diffuseness parameters of the nuclei in the DNS. The values employed in our calculations are within the range  $r_{0L,0H} = 1.0\text{--}1.16 \text{ fm}$  for the nuclear radii  $R_{L,H} = r_{0L,0H}A_{L,H}^{1/3}$  and within the range  $a_{L,H} = 0.47\text{--}0.56 \text{ fm}$  for the diffuseness parameters, depending on nuclear mass. The values of  $a_L$  and  $r_{0L}$  linearly increase from 0.47 and 1 fm for  ${}^4\text{He}$  to 0.56 and 1.16 fm for  ${}^{40}\text{Ar}$ , respectively, and then remain unchanged for heavier nuclei. These parameters allow us to describe well the heights and positions of the Coulomb barriers in many reactions.

For the calculation of the mass parameter in  $\eta_Z$ , we use the results of Ref. [52], where the expression

$$(B^{-1})_{\eta_Z} = \frac{1}{2m_0} \frac{A_{\text{neck}}}{2\sqrt{2\pi}b^2A^2} \quad (10)$$

was derived. Here  $b$  characterizes the DNS neck size,  $m_0$  is the nucleon mass, and

$$A_{\text{neck}} = \int [\rho_L(\mathbf{r}) + \rho_H(\mathbf{R} - \mathbf{r})] \exp\left(-\frac{z^2}{b^2}\right) d\mathbf{r}$$

is the number of nucleons in the neck region between two nuclei. In the present calculations, we set the neck parameter  $b = 0.479 - 0.019\eta_Z \text{ fm}$ , which corresponds to about three to five nucleons in the neck region. A slightly larger  $b$  for the symmetric DNS reflects a larger number of nucleons in the neck region between two heavy nuclei.

### A. Spectroscopic factor

To solve Eq. (3) and find  $S_L$ , it is convenient to replace  $\eta_Z$  by

$$x = 2\frac{Z_L}{Z} = 1 - \eta_Z.$$

This replacement of variables preserves the form of Eq. (3) with changing the scope of the definition for the function  $\Psi(x)$  to  $x \in [0, 1]$ , where  $x = 0$  corresponds to the state of the mononucleus, and  $x = 1$  is for the symmetric DNS configuration.

The values of  $U$  and  $(B^{-1})_{\eta_Z}$  are extended to the segments of the width  $2\Delta = 2/Z$  so that the points  $x$  are placed in the middle of the corresponding segments. The only exceptions are the mononucleus, for which we set  $x \in [0, 4\Delta)$ , and the  $\alpha$  particle with  $x \in [4\Delta, 5\Delta)$ . The representation of  $U$  and  $(B^{-1})_{\eta_Z}$  as step functions allows us to solve Eq. (3) by replacing it by the system of equations

$$-\frac{\hbar^2}{2}(B_j^{-1})_{\eta_Z} \frac{\partial^2}{\partial x^2} \psi_j(x) + U_j \psi_j(x) = E \psi_j(x). \quad (11)$$

which can be easily solved for each interval of  $x$ .

Then the normalized wave function

$$\int_0^1 |\Psi(x)|^2 dx = 1$$

is used for the definition of preformation probability  $S_L$  of the DNS with a certain charge number  $Z_L$  of the light cluster:

$$S_L = \int_{\eta_Z(Z_L)-\Delta}^{\eta_Z(Z_L)+\Delta} |\Psi(\eta_Z)|^2 d\eta_Z. \quad (12)$$

As shown in Refs. [36,37], the spectroscopic factors  $S_L$  calculated with Eq. (12) are in line with the spectroscopic factor of the microscopic description [22,26].

In the case of SF, we suppose that all DNS configurations in the SF region contribute ( $P_L = 1$ ). Therefore, the spectroscopic factor  $S_{\text{SF}}$  for SF is calculated as follows:

$$S_{\text{SF}} = \int_0^{\eta_{Ze}} |\Psi(\eta_Z)|^2 d\eta_Z, \quad (13)$$

where  $\eta_{Ze}$  is the exit turning point (Fig. 1).

### B. Half-lives

To compare the model results with the experimental ones, the half-lives are calculated as

$$T_{1/2} = \frac{\hbar \ln 2}{\Gamma_L} = \frac{\pi \ln 2}{\omega_0 S_L P_L}, \quad (14)$$

where the penetration probability  $P_L$  through the Coulomb barrier is calculated in the one-dimensional WKB approximation:

$$P_L = \left( 1 + \exp \left[ \frac{2}{\hbar} \int_{R_m}^{R_e} \sqrt{2\mu[V(R, \eta_Z(Z_L)) - Q]} dR \right] \right)^{-1},$$

where  $R_m$  and  $R_e$  are the positions of potential energy minima and exit point, respectively, and  $Q$  is the decay energy. The tip-tip orientation of nuclei is taken to calculate  $V(R, \eta_Z(Z_L))$ . For SF,  $S_L = S_{\text{SF}}$  and  $P_L = 1$  in Eq. (14).

## III. CALCULATED RESULTS

As shown in Figs. 1–4, the driving potential  $U$  contains the global maximum and minimum as a function of charge asymmetry. The energy of the initial fissioning nucleus (mononucleus) at  $x = 0$  ( $\eta_Z = 1$ ) is larger than the potential energies around the minimum at  $1 - \eta_Z > 0.6$ . To undergo fission, the nucleus needs to overcome the potential barrier in the charge asymmetry and be in the energy-resolved region at  $x > 0.6$ . Thus, the energy-resolved DNS configurations appear in the SF.

The calculated SF and  $\alpha$ -decay half-lives are presented in Fig. 5. The theoretical results are in quite good agreement with the experimental data. For the SF ( $\alpha$  decay) of  ${}^{232}\text{Th}$ ,  $T_{1/2} = 1.75 \times 10^{28} \text{ s}$  ( $T_{1/2} = 3.73 \times 10^{17} \text{ s}$ ), while the experimental half-life is  $T_{1/2} = 4 \times 10^{28} \text{ s}$  ( $T_{1/2} = 4.42 \times 10^{17} \text{ s}$ ). For the SF, the largest differences, factors of about 30 and 8, are obtained for  ${}^{234}\text{U}$  and  ${}^{238}\text{Pu}$ , respectively. However, this is acceptable for the model without adjustment of the parameters, which were set the same for all nuclei considered. The calculations reproduce the isotopic trends of  $T_{1/2}$  for SF, the enhanced stability at  $N = 152$  for Fm and No, and a rather weak dependence of  $T_{1/2}$  on  $N$  at  $N = 152$  for Rf and Sg [Fig. 5(b)]. We predict long SF half-lives for Sg and Hs at  $N = 164$ . The values of  $T_{1/2}$  are almost comparable

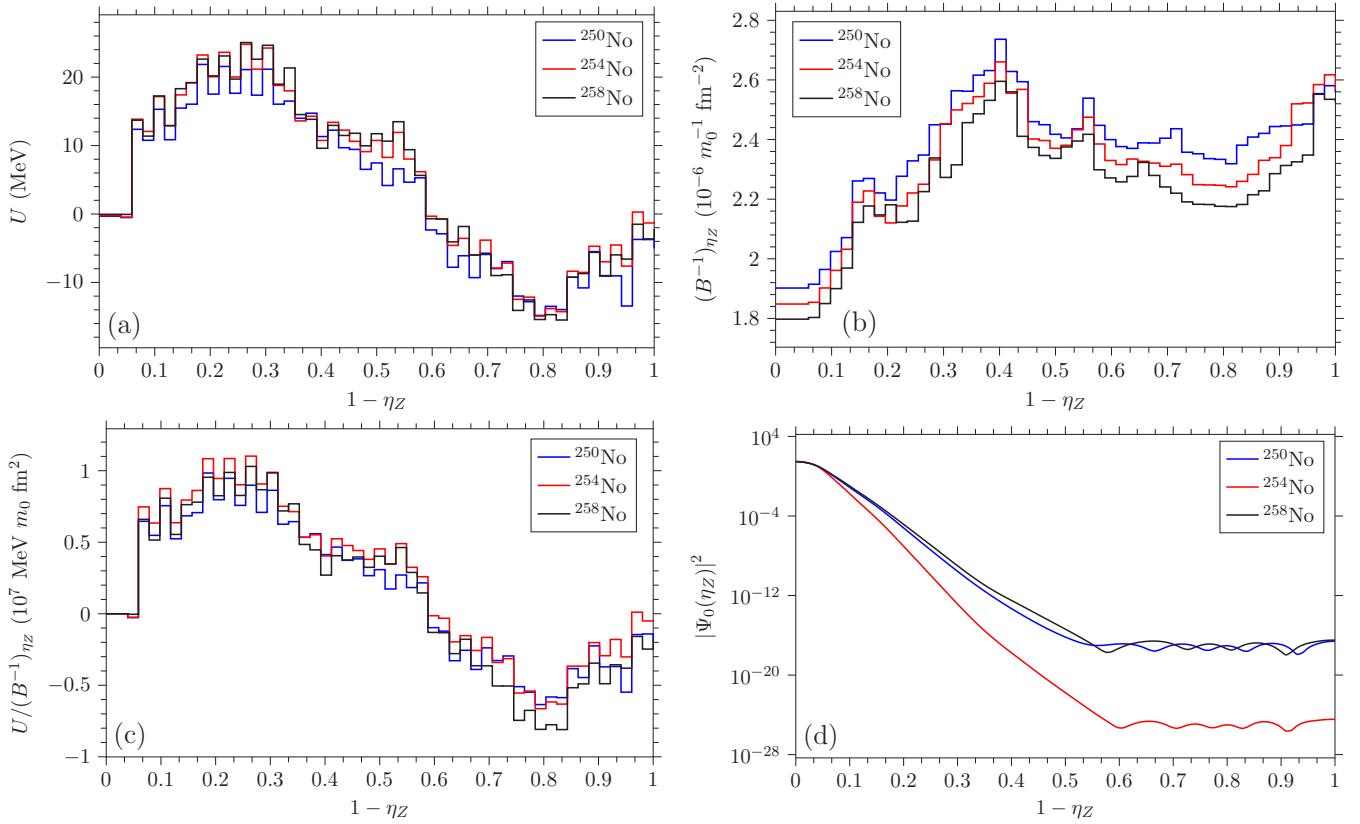


FIG. 2. Calculated driving potential  $U$  (a), inverse mass parameter  $(B^{-1})_{\eta_Z}$  (b), and ratio  $U/(B^{-1})_{\eta_Z}$  (c) as step functions of  $1 - \eta_Z$  for  $^{250,254,258}\text{No}$ . For these isotopes, the squares of the module of the ground-state wave functions  $|\Psi_0|^2$  (d) are also shown. The tip-tip orientation of nuclei is taken in the DNS.

for  $^{270}\text{Hs}$  ( $N = 162$ ) and  $^{272}\text{Hs}$  ( $N = 164$ ) and differ by less than 3 times for  $^{268}\text{Sg}$  ( $N = 162$ ) and  $^{270}\text{Sg}$  ( $N = 164$ ). The existing fission models [14–17] predict the maximum of  $T_{1/2}$  at  $N = 162$ . In our model, the absolute values of  $T_{1/2}$  for SF of  $^{268,270}\text{Sg}$  and  $^{270,272}\text{Hs}$  nuclei are many orders of magnitude smaller than those in the self-consistent fission model [15]. Note that for Sg and Hs stabilization against  $\alpha$ -decay occurs at  $N = 162$  (Fig. 5).

The potential barrier penetrability  $S_{\text{SF}}$  in the charge asymmetry coordinate can be calculated in the one-dimensional Wentzel-Kramers-Brillouin (WKB) approximation in accordance with the following formula:

$$S_{\text{SF}} = \left( 1 + \exp \left[ \frac{2}{\hbar} \int_{\eta_{Z0}}^{\eta_{Ze}} \sqrt{2U(R, \eta_Z, \Omega)/(B^{-1})_{\eta_Z}} d\eta_Z \right] \right)^{-1},$$

where  $\eta_{Z0}$  is the entrance turning point. As seen in Fig. 6, the exact and approximate WKB penetrabilities  $S_{\text{SF}}$  have the same isotopic dependencies, and their absolute values are either the same or differ for some nuclei up to two orders of magnitude. The difference between the exact and approximate calculations arises from the nonmonotonic dependencies of the driving potential and the mass parameter. As seen below, these two factors play an important role in the penetration process. For example, in the case of a larger barrier and a smaller mass parameter, the wave function may penetrate

more easily than in the case of a smaller barrier and a larger mass parameter.

The important role of the mass parameter can also be understood based on the results of calculations presented in Fig. 7: The replacement of the real mass parameters in nuclei  $^{252}\text{Fm}$  and  $^{256}\text{Rf}$  by the mass parameter for  $^{254}\text{No}$  in the calculations leads to an increase of  $T_{1/2}$  by about 2 orders of magnitude for  $^{252}\text{Fm}$  and a decrease of  $T_{1/2}$  by about 3 orders of magnitude for  $^{256}\text{Rf}$ .

For the fissioning nuclei  $^{252}\text{Fm}$ ,  $^{250,254,258}\text{No}$ , and  $^{254,256,262}\text{Rf}$ , the inverse mass parameters  $(B^{-1})_{\eta_Z}$  and the ratios  $U/(B^{-1})_{\eta_Z}$  as functions of  $1 - \eta_Z$  are presented in Figs. 2–4 together with the driving potentials  $U$ . It should be noted that the global maxima of  $U$  and  $(B^{-1})_{\eta_Z}$  are offset relative each other, with the maxima at about  $1 - \eta_Z = 0.3$  and  $0.4$  for  $U$  and  $(B^{-1})_{\eta_Z}$ , respectively. As clearly seen in Figs. 2 and 3, the isotopes of No or Rf differ in  $U/(B^{-1})_{\eta_Z}$  and, thus, in the wave functions  $|\Psi_0(1 - \eta_Z > 0.6)|^2$ , values of  $S_{\text{SF}}$  and half-lives  $T_{1/2}$ . In the case of isotopes  $^{250,254,258}\text{No}$ , at  $1 - \eta_Z > 0.6$  we have on average

$$\begin{aligned} U(^{254}\text{No}) &> U(^{250,258}\text{No}), \\ (B^{-1})_{\eta_Z}(^{250}\text{No}) &> (B^{-1})_{\eta_Z}(^{254}\text{No}) > (B^{-1})_{\eta_Z}(^{258}\text{No}), \\ \frac{U}{(B^{-1})_{\eta_Z}}(^{254}\text{No}) &> \frac{U}{(B^{-1})_{\eta_Z}}(^{250,258}\text{No}), \end{aligned}$$

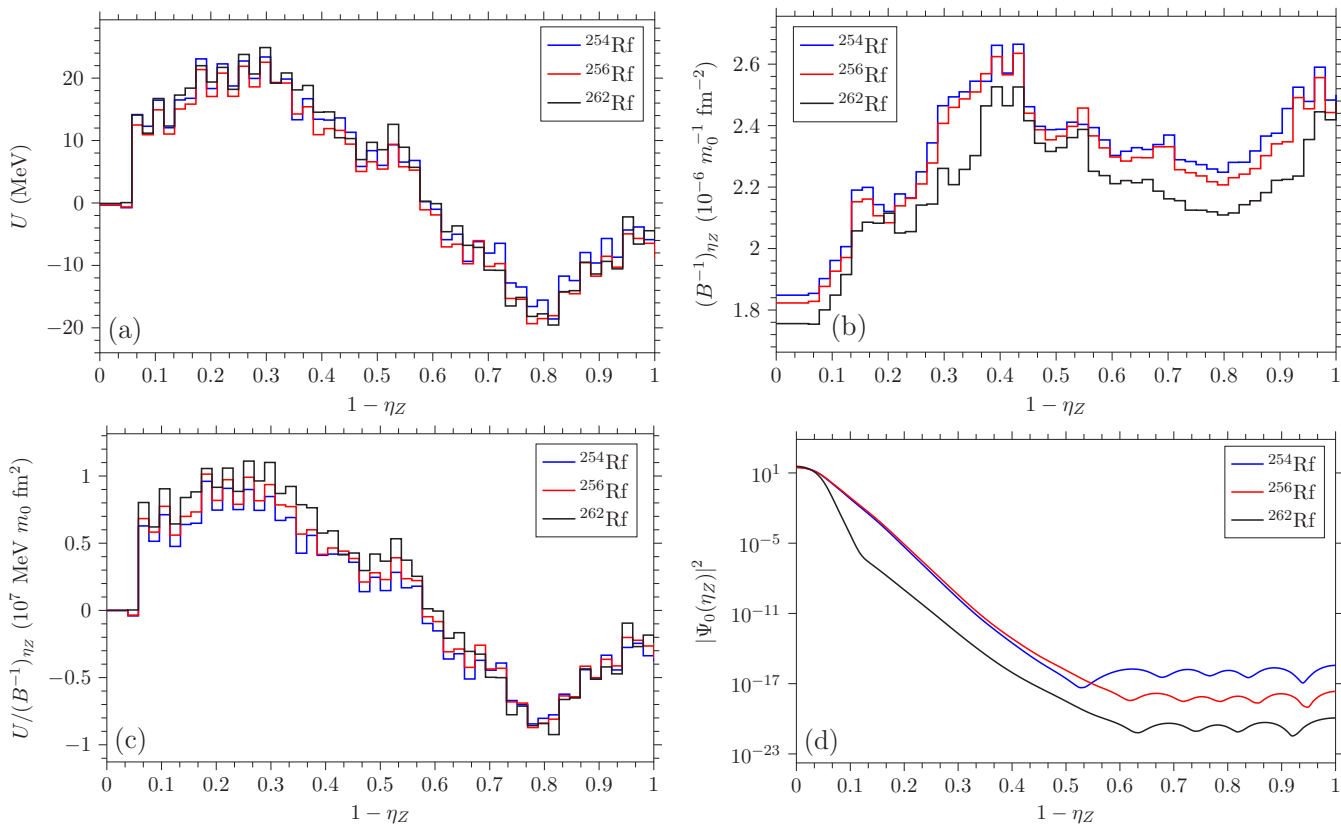


FIG. 3. The same as in Fig. 2, but for  $^{254,256,262}\text{Rf}$ .

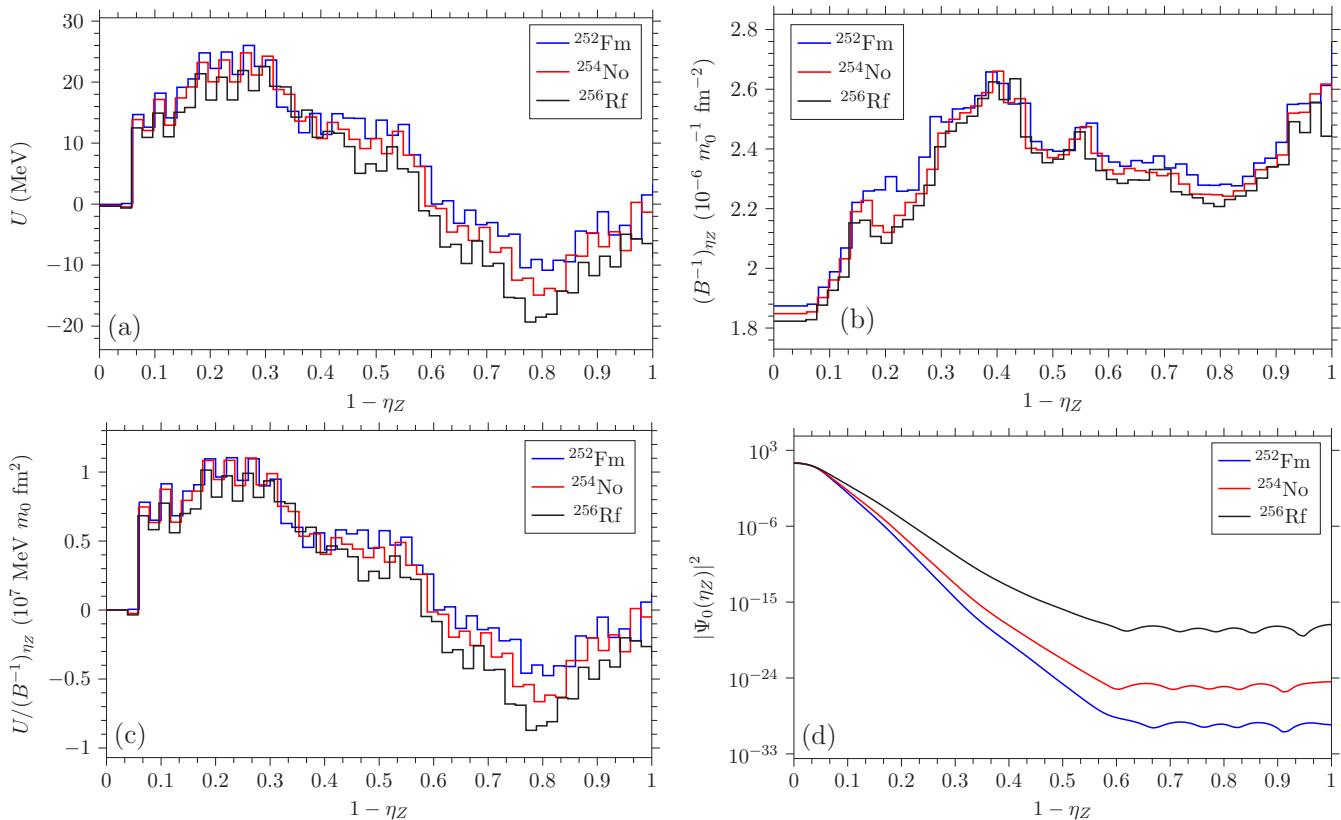


FIG. 4. The same as in Fig. 2, but for  $^{252}\text{Fm}$ ,  $^{254}\text{No}$ , and  $^{256}\text{Rf}$ .

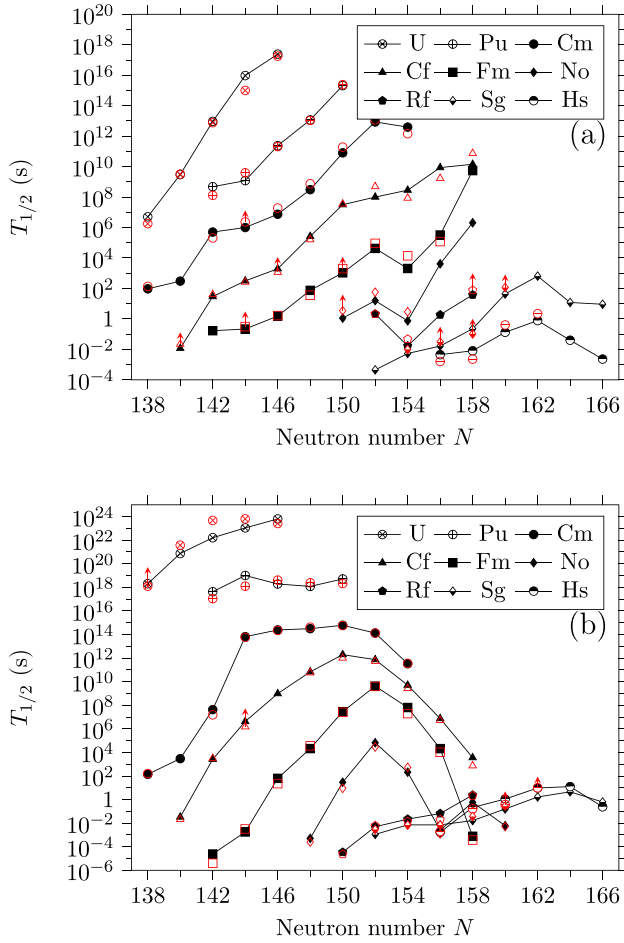


FIG. 5. Calculated and experimental  $\alpha$ -decay (a) and SF (b) half-lives of the even isotopes of U, Pu, Cm, Cf, Fm, No, Rf, Sg, and Hs. Symbols connected by lines represent theoretically calculated results; red open symbols represent the experimental data [53–57]. Arrows indicate the lower limits of half-lives.

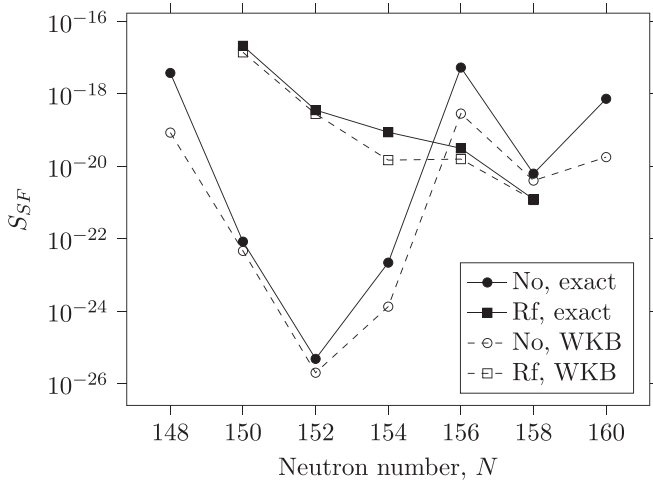


FIG. 6. Calculated exact [from the solution of Eq. (3), symbols connected by solid lines] and approximate WKB (open symbols connected by dashed lines) values of  $S_{SF}$  for the isotopes of No (closed circles) and Rf (closed squares). The tip-tip orientation of nuclei is taken in the DNS.

and

$$|\Psi_0(^{254}\text{No})|^2 < |\Psi_0(^{250,258}\text{No})|^2.$$

As a result, the maximum half-life  $T_{1/2}$  corresponds to  $^{254}\text{No}$  with a neutron closed subshell at  $N = 152$  (Fig. 5). Note that the barrier heights  $U_b$  in Fig. 8 are related by the following inequalities:

$$U_b(^{250}\text{No}) < U_b(^{254}\text{No}) < U_b(^{258}\text{No}),$$

which mean that the fission barrier is not the highest in  $^{254}\text{No}$ .

As seen in Fig. 8, the rapid growth of  $U_b$  from  $^{250}\text{No}$  ( $N = 148$ ) to  $^{254}\text{No}$  ( $N = 152$ ) correlates with a sharp increase in  $T_{1/2}$ . The growth of  $U_b$  slows down from  $^{254}\text{No}$  ( $N = 152$ ) to  $^{258}\text{No}$  ( $N = 156$ ). However, this leads to the reduction of  $T_{1/2}$  with increasing  $N$ . From  $^{258}\text{No}$  to  $^{260}\text{No}$ , again, the rate of increase in  $U_b$  rises, which leads to a maximum of  $T_{1/2}$  at  $N = 158$ . In the case of Fm isotopes, there is a constant drop of  $T_{1/2}$  at  $N > 152$  although  $U_b$  increases from  $N = 154$  to  $N = 156$  (Fig. 8).

For the fissioning isotopes of Rf, we have on average the following at  $1 - \eta_Z > 0.6$ :

$$U(^{262}\text{Rf}) > U(^{254}\text{Rf}) > U(^{256}\text{Rf}),$$

$$(B^{-1})_{\eta_Z}(^{254}\text{Rf}) > (B^{-1})_{\eta_Z}(^{256}\text{Rf}) > (B^{-1})_{\eta_Z}(^{262}\text{Rf}),$$

$$\frac{U}{(B^{-1})_{\eta_Z}}(^{262}\text{Rf}) > \frac{U}{(B^{-1})_{\eta_Z}}(^{256}\text{Rf}) > \frac{U}{(B^{-1})_{\eta_Z}}(^{254}\text{Rf}),$$

and

$$|\Psi_0(^{262}\text{Rf})|^2 < |\Psi_0(^{256}\text{Rf})|^2 < |\Psi_0(^{254}\text{Rf})|^2.$$

Thus, the known heaviest isotope  $^{262}\text{Rf}$  has the highest half-life. In Fig. 8, we observe a rather sharp growth of  $U_b$  from  $^{256}\text{Rf}$  to  $^{262}\text{Rf}$ .

As another example, in Fig. 4 we compare the driving potentials and inverse mass parameter of nuclei  $^{252}\text{Fm}$ ,  $^{254}\text{No}$ , and  $^{256}\text{Rf}$  with  $N = 152$ . At  $1 - \eta_Z > 0.6$  we have on average

$$U(^{252}\text{Fm}) > U(^{254}\text{No}) > U(^{256}\text{Rf}),$$

$$(B^{-1})_{\eta_Z}(^{252}\text{Fm}) > (B^{-1})_{\eta_Z}(^{254}\text{No}) > (B^{-1})_{\eta_Z}(^{256}\text{Rf}),$$

$$\frac{U}{(B^{-1})_{\eta_Z}}(^{252}\text{Fm}) > \frac{U}{(B^{-1})_{\eta_Z}}(^{254}\text{No}) > \frac{U}{(B^{-1})_{\eta_Z}}(^{256}\text{Rf}),$$

$$w_{\eta_Z}(^{252}\text{Fm}) > w_{\eta_Z}(^{254}\text{No}) > w_{\eta_Z}(^{256}\text{Rf}),$$

and

$$|\Psi_0(^{252}\text{Fm})|^2 < |\Psi_0(^{254}\text{No})|^2 < |\Psi_0(^{256}\text{Rf})|^2.$$

As a result,

$$T_{1/2}(^{252}\text{Fm}) > T_{1/2}(^{254}\text{No}) > T_{1/2}(^{256}\text{Rf}).$$

As follows from Fig. 4, the energy-resolved region to the right of the barrier becomes deeper and wider with increasing atomic number of the fissioning nucleus. This results in a narrowing of the width  $w_{\eta_Z} = \eta_{Z0} - \eta_{Ze}$  of the potential barrier (Fig. 8) and a decrease of the value of  $T_{1/2}$  (Fig. 5).

Dependence of the  $Q$  value of fragmentation, corresponding to the top of the potential barrier in  $\eta_Z$ , on the neutron number of the fissioning nucleus is shown in Fig. 8. For

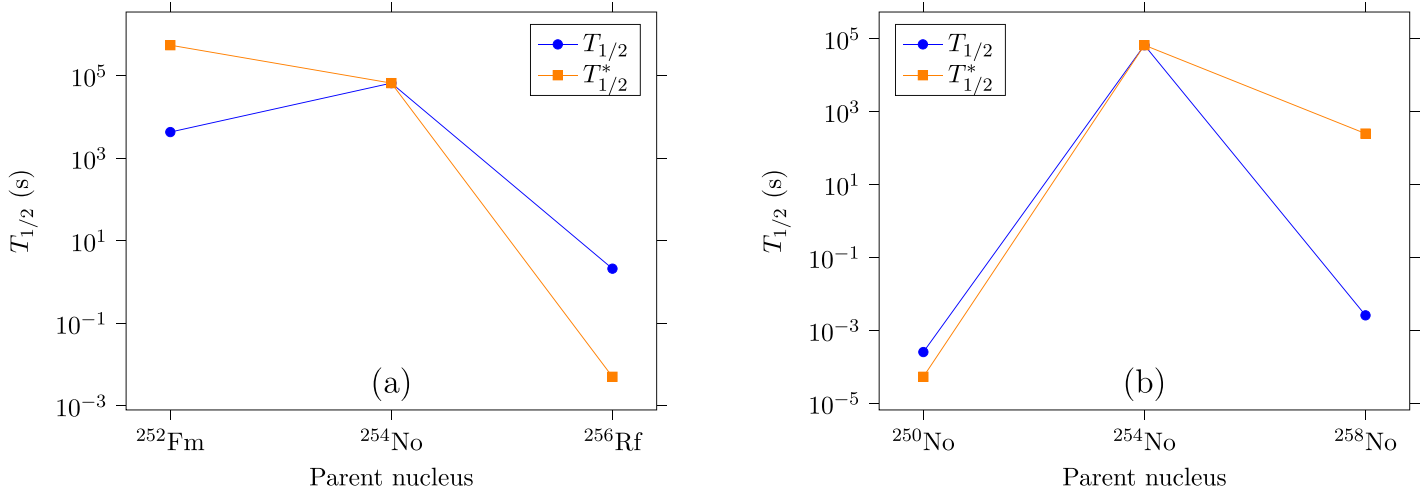


FIG. 7. Calculated SF half-lives  $T_{1/2}$  (closed circles connected by solid lines) for  $^{252}\text{Fm}$ ,  $^{254}\text{No}$ , and  $^{256}\text{Rf}$  and for  $^{250,254,258}\text{No}$ . Closed squares connected by solid lines denote the half-lives  $T_{1/2}^*$  calculated with the inverse mass parameter in  $^{254}\text{No}$  for all other nuclei.

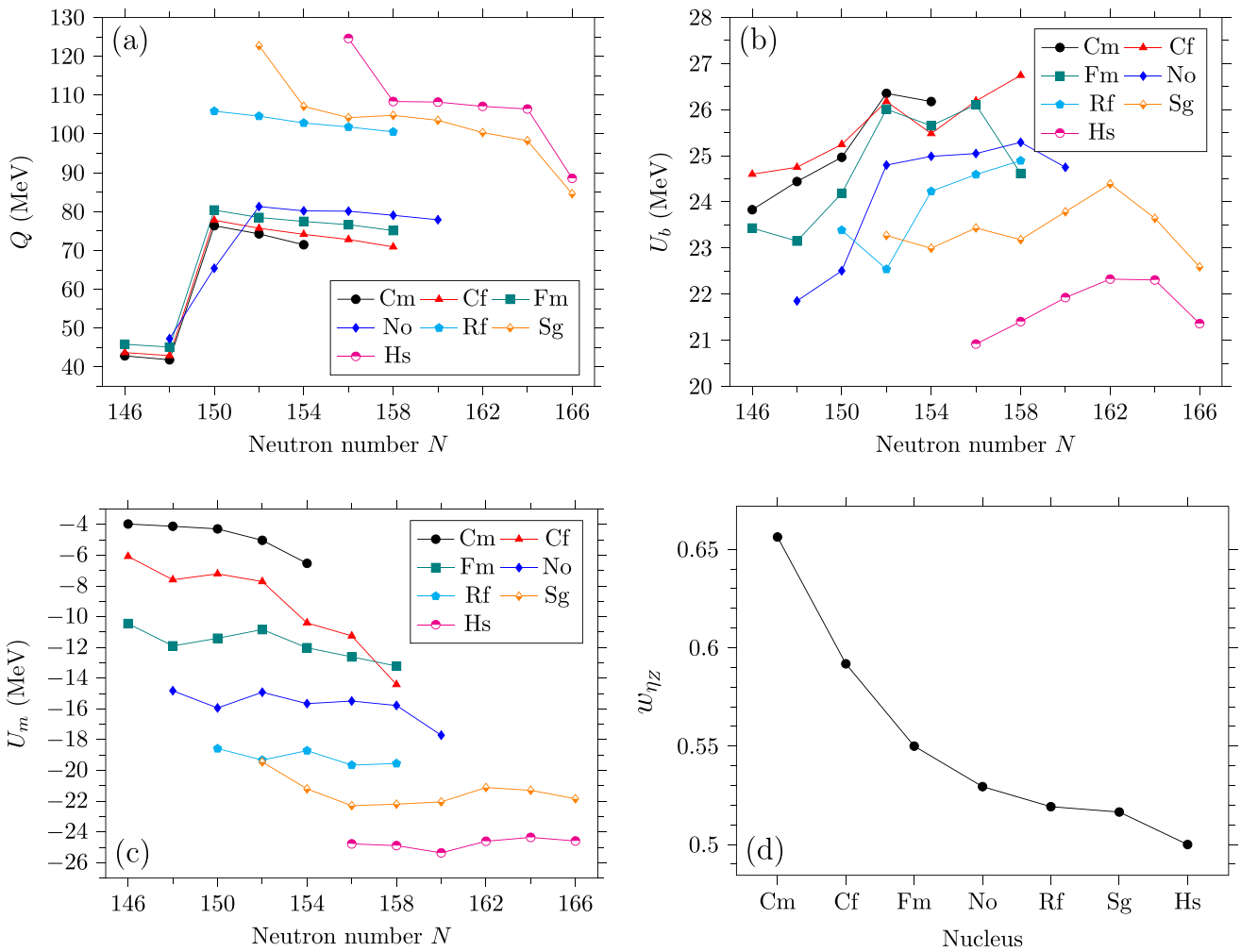


FIG. 8. The  $Q$  values at the top of the potential barrier in  $\eta_Z$  (a), the heights  $U_b$  of the potential barriers in  $\eta_Z$  (b), the depths  $U_m$  of the global minima in the driving potential (c), and the average width  $w_{\eta_Z} = \eta_{Z0} - \eta_{Ze}$  (d) of the potential barrier for the even isotopes of U, Pu, Cm, Cf, Fm, No, Rf, Sg, and Hs. The characteristics of the potential are explained in Fig. 1.

TABLE I. Calculated ( $T_{1/2}^{\text{th}}$ ) and experimental ( $T_{1/2}^{\text{exp}}$ ) CR half-lives for the indicated actinides.

Decay mode	$T_{1/2}^{\text{th}}$ (s)	$T_{1/2}^{\text{exp}}$ (s)	Decay mode	$T_{1/2}^{\text{th}}$ (s)	$T_{1/2}^{\text{exp}}$ (s)
$^{232}\text{U} \rightarrow ^{24}\text{Ne}$	$4.07 \times 10^{21}$	$1.89 \times 10^{21}$	$^{236}\text{Pu} \rightarrow ^{28}\text{Mg}$	$2.06 \times 10^{21}$	$4.67 \times 10^{21}$
$^{234}\text{U} \rightarrow ^{26}\text{Ne}$	$1.29 \times 10^{25}$	$1.20 \times 10^{25}$	$^{238}\text{Pu} \rightarrow ^{30}\text{Mg}$	$2.79 \times 10^{25}$	$5.01 \times 10^{25}$
$^{236}\text{U} \rightarrow ^{28}\text{Mg}$	$4.33 \times 10^{25}$	$3.47 \times 10^{25}$	$^{238}\text{Pu} \rightarrow ^{32}\text{Si}$	$5.15 \times 10^{25}$	$1.99 \times 10^{25}$
$^{238}\text{U} \rightarrow ^{30}\text{Mg}$	$1.85 \times 10^{26}$	$1.89 \times 10^{26}$	$^{242}\text{Cm} \rightarrow ^{34}\text{Si}$	$2.09 \times 10^{23}$	$1.41 \times 10^{23}$

the nuclei with  $Z < 103$ , the  $Q$  value sharply increases from  $N = 148$  up to  $N = 150$  or  $152$ , and then weakly decreases. For the nuclei Rf and Sg (Hs), the  $Q$  value weakly decreases from  $N = 150$  up to  $N = 158$  and from  $N = 154$  up to  $N = 164$  (from  $N = 158$  up to  $N = 164$ ), respectively. The overall growth of the  $Q$  value with  $Z$  is visible, which leads to a general decrease of the height  $U_b$  of the barrier with increasing  $Z$ . From a comparison of Figs. 5 and 8, one can see that a sharp change in the  $Q$  value between the groups of U–No and Rf–Hs correlates with the changes in the functional dependence of  $T_{1/2}$  on  $N$  and in the absolute values of  $T_{1/2}$ . A sharp (of about 20 MeV) jump in the  $Q$  value from  $^{254}\text{No}$  to  $^{256}\text{Rf}$  is mainly responsible for a sharp decrease of  $U_b$  and, correspondingly,  $T_{1/2}$ .

To verify the model, the half-lives with respect to CR are calculated and compared with experimental data [53] for even U, Pu, and Cm isotopes (Table I). Good agreement is obtained between the calculated and experimental half-lives without any special adjustment of parameters. Note that the maximal deviation from the experimental half-lives is within a factor of 6.

Besides a good description of half-lives with respect to  $\alpha$  decay, CR, and SF for  $^{256}\text{No}$ , we predict  $T_{1/2}^{\text{th}}(^{256}\text{No} \rightarrow ^{48}\text{Ca}) = 3.86 \times 10^{11}$  s for the emission of  $^{48}\text{Ca}$  in this nucleus. Note that the experimental  $\alpha$  decay ( $T_{1/2} = 2.91$  s) and SF ( $T_{1/2} = 549$  s) half-lives are much less than this prediction.

#### IV. SUMMARY

The DNS model (cluster approach) reproduces the global isotopic trends of SF and  $\alpha$ -decay half-lives for even nuclei U, Pu, Cm, Cf, Fm, No, Rf, Sg, and Hs. In contrast to the existing fission models, our model gives correct absolute values for  $T_{1/2}$  of SF, CR, and  $\alpha$  decay assuming charge

(mass) asymmetry as a relevant collective variable responsible for these processes. In terms of SF ( $\alpha$ -decay) half-lives, the model presented describes well the values, which differ up to 34 (20) orders of magnitude. Larger values of SF half-lives at  $N = 152$  are well described. So the basic assumption of the model on the collective coordinate that is responsible for the  $\alpha$  decay, CR, and SF seems to be correct. For both Sg and Hs, our results indicate stabilization against SF towards the deformed neutron shell at  $N = 164$  whereas stabilization against  $\alpha$  decay occurs at  $N = 162$ . As demonstrated, a drastic change in the  $Q$  value of binary fragmentation, corresponding to the top of the potential barrier in  $\eta_Z$ , in the U–No and Rf–Hs nuclear groups correlates with the changes in the functional dependence of SF half-life  $T_{1/2}$  on the neutron number  $N$  and in the absolute values of  $T_{1/2}$ .

We have found that the effects of the shape of the potential barrier (i.e., the width) and inertia parameter for the fission are significant, and therefore these characteristics are as important as the height of the potential barrier. Thus, the fission half-lives do not allow us to make an unambiguous conclusion about the height of the potential barriers. Note that the height of the potential barriers in  $\eta_Z$  is much larger than the height of the barriers along the elongation of the fissioning nucleus in macroscopic-microscopic and self-consistent mean-field fission models. Another important point is that in the model presented SF is described by the same collective coordinates as complete fusion in the DNS approach [45].

#### ACKNOWLEDGMENTS

This work was partly supported by the Ministry of Science and Higher Education of the Russian Federation (Contract No. 075-10-2020-117).

- |  |  |
|--|--|
| <p>[1] Yu. Ts. Oganessian, Yu. P. Tretyakov, A. S. Iljinov, A. G. Demin, A. A. Pleve, S. P. Tretyakova, V. M. Plotko, M. P. Ivanov, N. A. Danilov, Yu. S. Korotkin, and G. N. Flerov, <i>JETP Lett.</i> <b>20</b>, 265 (1974).</p> <p>[2] Yu. Ts. Oganessian, A. S. Iljinov, A. G. Demin, and S. P. Tretyakova, <i>Nucl. Phys. A</i> <b>239</b>, 353 (1975).</p> <p>[3] A. Türler, H. Gaeggeler, D. T. Jost, P. Armbruster, W. Bröchle, H. Folger, F. P. Hessberger, S. Hofmann, G. Münzenberg, V. Ninov, M. Schädel, K. Sümmerer, J. V. Kratz, and V. W. Scherer, <i>Z. Phys. A</i> <b>331</b>, 363 (1988).</p> <p>[4] F. P. Hessberger <i>et al.</i>, <i>Z. Phys. A</i> <b>359</b>, 415 (1997).</p> <p>[5] S. Hofmann and G. Münzenberg, <i>Rev. Mod. Phys.</i> <b>72</b>, 733 (2000).</p> | <p>[6] F. P. Hessberger, <i>Eur. Phys. J. A</i> <b>53</b>, 75 (2017).</p> <p>[7] J. Randrup, S. E. Larsson, P. Möller, S. G. Nilsson, K. Pomorski, and A. Sobiczewski, <i>Phys. Rev. C</i> <b>13</b>, 229 (1976).</p> <p>[8] E. K. Hulet <i>et al.</i>, <i>Phys. Rev. Lett.</i> <b>56</b>, 313 (1986).</p> <p>[9] S. Ćwiok, P. Rozmej, A. Sobiczewski, and Z. Patyk, <i>Nucl. Phys. A</i> <b>491</b>, 281 (1989).</p> <p>[10] P. Möller, J. R. Nix, and W. J. Swiatecki, <i>Nucl. Phys. A</i> <b>492</b>, 349 (1989).</p> <p>[11] Yu. Ts. Oganessian, <i>J. Phys. G</i> <b>34</b>, R165 (2007).</p> <p>[12] Yu. Ts. Oganessian and V. K. Utyonkov, <i>Nucl. Phys. A</i> <b>944</b>, 62 (2015); <i>Rep. Prog. Phys.</i> <b>78</b>, 036301 (2015).</p> <p>[13] S. Hofmann, <i>Radiochim. Acta</i> <b>99</b>, 405 (2011).</p> |
|--|--|

- [14] R. Smolanczuk, J. Skalski, and A. Sobiczewski, *Phys. Rev. C* **52**, 1871 (1995); R. Smolanczuk, *ibid.* **56**, 812 (1997).
- [15] M. Warda and J. L. Egidio, *Phys. Rev. C* **86**, 014322 (2012).
- [16] A. Staszczak, A. Baran, and W. Nazarewicz, *Phys. Rev. C* **87**, 024320 (2013).
- [17] R. Rodríguez-Guzmán and L. M. Robledo, *Phys. Rev. C* **98**, 034308 (2018); R. Rodríguez-Guzmán, Y. M. Humadi, and L. M. Robledo, *Eur. Phys. J. A* **56**, 43 (2020).
- [18] H. J. Fink, W. Scheid, and W. Greiner, *J. Phys. G* **1**, 685 (1975).
- [19] H. J. Fink, J. A. Maruhn, W. Scheid, and W. Greiner, *Z. Phys.* **268**, 321 (1974).
- [20] J. A. Maruhn, W. Scheid, and W. Greiner, in *Heavy Ion Collisions*, edited by R. Bock (North Holland, Amsterdam, 1980), Vol. 2, p. 399.
- [21] R. K. Gupta, S. Singh, R. K. Puri, and W. Scheid, *Phys. Rev. C* **47**, 561 (1993).
- [22] Yu. M. Tchuvil'sky, *Cluster Radioactivity* (Moscow State University, Moscow, 1997).
- [23] W. Greiner, M. Ivascu, D. N. Poenaru, and A. Sandulescu, in *Treatise on Heavy Ion Science*, edited by D. A. Bromley (Plenum, New York, 1989), Vol. 8, p. 641.
- [24] D. N. Poenaru *et al.*, *At. Data Nucl. Data Tables* **34**, 423 (1986); **48**, 231 (1991).
- [25] Yu. S. Zamyatin, V. L. Mikheev, S. P. Tretyakova, V. I. Furman, S. G. Kadmsky, and Y. M. Chuvil'skii, *Sov. J. Part. Nucl.* **21**, 231 (1990).
- [26] S. G. Kadmsky, S. D. Kurgalin, and Yu. M. Tchuvil'sky, *Phys. Part. Nucl.* **38**, 699 (2007).
- [27] D. N. Poenaru, *Nuclear Decay Modes* (IOP, Bristol, 1996).
- [28] D. N. Poenaru and R. A. Gherghescu, *Eur. Phys. Lett.* **124**, 52001 (2018); **118**, 22001 (2017).
- [29] K. Varga, R. G. Lovas, and R. J. Liotta, *Phys. Rev. Lett.* **69**, 37 (1992).
- [30] N. Itagaki, J. Cseh, and M. Ploszajczak, *Phys. Rev. C* **83**, 014302 (2011).
- [31] J. Cseh, A. Algora, J. Darai, and P. O. Hess, *Phys. Rev. C* **70**, 034311 (2004).
- [32] W. Sciani, Y. Otani, A. Lépine-Szily, E. A. Benjamim, L. C. Chamon, R. L. Filho, J. Darai, and J. Cseh, *Phys. Rev. C* **80**, 034319 (2009).
- [33] J. Cseh, J. Darai, W. Sciani, Y. Otani, A. Lépine-Szily, E. A. Benjamim, L. C. Chamon, and R. L. Filho, *Phys. Rev. C* **80**, 034320 (2009).
- [34] D. Lebhertz *et al.*, *Phys. Rev. C* **85**, 034333 (2012).
- [35] A. Algora, J. Cseh, J. Darai, and P. O. Hess, *Phys. Lett. B* **639**, 451 (2006).
- [36] S. N. Kuklin, G. G. Adamian, and N. V. Antonenko, *Yad. Fiz.* **68**, 1501 (2005) [*Phys. At. Nucl.* **68**, 1443 (2005)].
- [37] S. N. Kuklin, G. G. Adamian, and N. V. Antonenko, *Phys. Rev. C* **71**, 014301 (2005).
- [38] S. N. Kuklin, G. G. Adamian, and N. V. Antonenko, *Yad. Fiz.* **71**, 1788 (2008) [*Phys. At. Nucl.* **71**, 1756 (2008)]; S. N. Kuklin, T. M. Shneidman, G. G. Adamian, and N. V. Antonenko, *Eur. Phys. J. A* **48**, 112 (2012).
- [39] V. V. Volkov, E. A. Cherepanov, and Sh.A. Kalandarov, *Phys. Part. Nucl. Lett.* **13**, 729 (2016).
- [40] T. M. Shneidman, G. G. Adamian, N. V. Antonenko, R. V. Jolos, and W. Scheid, *Phys. Lett. B* **526**, 322 (2002); *Phys. Rev. C* **67**, 014313 (2003).
- [41] G. G. Adamian, N. V. Antonenko, R. V. Jolos, and T. M. Shneidman, *Phys. Rev. C* **70**, 064318 (2004).
- [42] G. G. Adamian, N. V. Antonenko, R. V. Jolos, Yu. V. Palchikov, and W. Scheid, *Phys. Rev. C* **67**, 054303 (2003).
- [43] G. G. Adamian, N. V. Antonenko, R. V. Jolos, Yu. V. Palchikov, W. Scheid, and T. M. Shneidman, *Phys. Rev. C* **69**, 054310 (2004).
- [44] T. M. Shneidman, G. G. Adamian, N. V. Antonenko, and R. V. Jolos, *Phys. Rev. C* **74**, 034316 (2006).
- [45] G. G. Adamian, N. V. Antonenko, and W. Scheid, *Clusters in Nuclei*, Vol. 2, edited by C. Beck, Lecture Notes in Physics Vol. 848 (Springer-Verlag, Berlin, 2012), p. 165.
- [46] I. S. Rogov, G. G. Adamian, and N. V. Antonenko, *Phys. Rev. C* **100**, 024606 (2019).
- [47] G. G. Adamian *et al.*, *Int. J. Mod. Phys. E* **5**, 191 (1996).
- [48] J. K. Tuli, *Nuclear Wallet Cards* (BNL, New York, 2000).
- [49] S. Raman *et al.*, *At. Data Nucl. Data Tables* **78**, 1 (2001).
- [50] P. Möller, A. J. Sierk, T. Ichikawa, and H. Sagawa, *At. Data Nucl. Data Tables* **109–110**, 1 (2016).
- [51] A. B. Migdal, *Theory of Finite Fermi Systems and Applications to Atomic Nuclei* (Nauka, Moscow, 1982; Interscience, New York, 1967).
- [52] G. G. Adamian, N. V. Antonenko, and R. V. Jolos, *Nucl. Phys. A* **584**, 205 (1995).
- [53] <http://www.nndc.bnl.gov/nndc/ensdf/>.
- [54] S. Hofmann *et al.*, *Eur. Phys. J. A* **10**, 5 (2001).
- [55] D. Ackermann, *Prog. Theor. Phys. Suppl.* **196**, 255 (2012).
- [56] K. Nishio *et al.*, *Phys. Rev. C* **82**, 024611 (2010).
- [57] Yu. Ts. Oganessian *et al.*, *Phys. Rev. C* **87**, 034605 (2013).